Closed-form solutions for axisymmetric FGM elastic plates

Giuseppe Ruta* and Isaac Elishakoff†

Abstract. Suitable, yet general enough, choices of functional grading along the radius and the thickness of axisymmetric circular plates may lead to closed-form solutions for the linear elastic direct problem. The plates are modelled according to the usual Kirchhoff-Love theory, since they are supposed thin; to abstract from actual values of geometric and material parameters, the governing equations are dealt with in non-dimensional form. Some instances are presented, along with thorough comments.

Keywords: Axisymmetric plates; FGM; closed-form solutions.

1. INTRODUCTION

The investigation on the behaviour of elastic circular plates of variable thickness and hence of variable flexural rigidity starts apparently with the paper by Garabedian of 1923 [1]. Then, books in the Russian language followed, namely those by Kitover in 1953 [2], Kovalenko in 1959 [3] and Birger in 1961 [4]. Before those, we may quote the paper by Olsson in 1937 [5], dealing with circular plates with exponentially variable thickness by resorting to degenerate hypergeometric functions. In 1944 Bisshopp [6] investigated circular plates with conical profile, always using hypergeometric functions. Kovalenko in [3] and Ando in [7] considered a special polynomial variation of the thickness, hence of the bending stiffness. Lord and Yousef [8] conducted both analytical and experimental studies on the subject of circular plates with variable stiffness. Biswas [9] studied the thermal deflection problem; Laura *et al.* [10] investigated the behaviour of circular plates elastically restrained along the edge. Han and Liew [11] studied the approximate method of differential quadrature element method (DQEM) for axisymmetric bending of thick circular plates.

* Associate Professor, Department of Structural and Geotechnical Engineering, University "La Sapienza", & National Group for Mathematical Physics, Rome, Italy; e-mail: giuseppe.ruta@uniroma1.it (corresponding author)
† Distinguished Research Professor, Ocean and Mechanical Engineering Department, Florida Atlantic University, Boca Raton, Florida, USA; e-mail: elishako@fau.edu

As far as functionally graded plates are concerned, the study of axisymmetric bending of functionally graded circular and annular plates was pioneered by Reddy *et al.* in their paper of 1999 [12]. Civalek and Ülker [13] resorted to the harmonic differential quadrature (HDQ) method to solve the relevant problems. Gunes and Aydin [14] studied functionally graded circular plates under a drop-weight. Farahani *et al.* [15] conducted the axisymmetric analysis of circular plates using the radial point interpolation method. Tseng and Tarn [16] furnished an exact elasticity solution for axisymmetric deformations of circular plates, whereas Karttunen *et al.* [17] provided exact, elasticity-based, finite element solutions. Shariyat and Alipour [18] conducted analytical bending and stress analysis of variable thickness FGM auxetic structures. Saidi *et al.* [19] conducted both axisymmetric bending and buckling analyses of thick functionally graded circular plates by resorting to unconstrained third-order shear deformation plate theory. Vivio and Vullo [20] derived the closed-form solutions of axisymmetric bending of circular plates having non-linear variable thickness. Alibeigloo and Simintan [21] derived elasticity-based solutions, whereas Rad and Behravan [22] dealt with static analysis of non-uniform 2D functionally graded auxetic-porous circular plates interacting with the gradient elastic foundations involving friction force. Yang *et al.* [23] dealt with FGM circular plates, whereas Belardi *et al.* used Galerkin's method [24], Ritz method [25, 26]. In the very recent paper [27] analytical solutions are looked for when the material properties are varied along the thickness. Purely numerical solutions are at ease by up-to-date finite elements codes, e.g., [28]. FGM circular plates were treated by semi-inverse method by Elishakoff et al. [29]. Exponential functional grading was investigated in [30] for the case of beams, i.e., in one-dimensional structural elements, and polynomial functional grading was considered in [31] for thin plates. A hint on the possibility to find closed-form solutions for the transverse behaviour of axisymmetric plates functionally graded along both radius and thickness is given in [32]. Actual technological realizations of functional grading and manufacturing techniques may be found, for instance, in the monographs [33, 34].

The present paper has a single objective: taking inspiration from [32], we wish to furnish closed-form solutions in both slab (i.e., in-plane) and transverse behaviour of elastic plates with variable

flexural rigidity owing to a functional grading in radial and transverse directions. That is, the material properties are supposed to be suitably varied, so that the plate in-plane and transverse stiffnesses vary accordingly, affecting the expressions of the governing equations in terms of displacement components. Closed-form solutions are found here by special functions such as Laguerre generalised polynomials, the confluent hypergeometric function, and the hypergeometric function.

These solutions can then serve as benchmarks in order to be able to judge the accuracy of approximate solutions, derived via the finite element method [17], Galerkin [24] or Ritz [25, 26] methods, not to mention the direct interest from the point of view of possible applications. Indeed, it is barely to remark how design and verification requires closed-form expressions.

The paper is organized as follows: after this introduction, we will present the field equations for the considered problem, recalling the so-called Kirchhoff-Love hypotheses for thin plates and assuming a multiplicative functional grading. In order to abstract from actual values of the geometrical and physical quantities dealt with, the governing equations and boundary conditions are turned into non-dimensional form. Then, the search for closed-form solutions for the slab behaviour is presented, followed by the corresponding search for the transverse behaviour. The closed-form expressions are accompanied by graphical representations and thorough comments. Final remarks conclude the work, summarizing the results and introducing new perspectives.

2. FIELD EQUATIONS

We consider bodies that in their reference state occupy a three-dimensional region of the Euclidean ambient space $\mathcal{E}$ consisting of a series of copies of a straight segment of length h. Each of these copies is attached at half its length to a point of a plane region (called middle surface), orthogonally to it. The middle surface is a circular crown bounded by inner and outer circumferences with the same centre and radii r_i, r_o respectively; in particular, if $r_i \to 0$ we describe solid, non-hollow, bodies. Let us pose that $h \ll r_i, r_o$, that is, the considered shapes are tablets, or thin straight cylinders. Moreover, let the changes in shape of these bodies be described by displacement components having magnitudes

much smaller than the radii r_i, r_o. Then, the bodies may be modelled as thin plates with the so-called Kirchhoff-Love inner constraint: the material fibres along the straight segments normal to the middle surface may be assumed to behave as rigid filaments clamped to the middle surface.

To describe the mechanical behaviour of the plates, we fix a polar frame with origin at the centre of the middle surface and radial, circumferential and transverse coordinates r, φ, z respectively. Then, the reference shape of the plate is the three-dimensional domain $\left\{(r,\varphi,z)\colon r_i \le r \le r_o, 0 \le \varphi < 2\pi, -\frac{h}{2} \le z \le \frac{h}{2}\right\}$; its boundary consists of the upper (superscript +) and lower (superscript $-$) bases $\mathcal{B}^{\pm} = \left\{(r,\varphi,z)\colon r_i < r < r_o, 0 \le \varphi < 2\pi, z = \pm\frac{h}{2}\right\}$ and of the inner (subscript i) and outer (subscript o) mantle $\mathcal{M}_{i,o} = \left\{(r,\varphi,z)\colon r = r_i, r_o, 0 \le \varphi < 2\pi, -\frac{h}{2} \le z \le \frac{h}{2}\right\}$.

The displacement components of the material points of the body superposed to the geometrical points of the reference shape are denoted by u, v, w along the radial, circumferential and transverse coordinates, respectively. Due to the supposed rigidity of the transverse filaments, they are given by

$$u(r,\varphi,z) = u_0(r,\varphi) + z\vartheta_\varphi(r,\varphi), \qquad v(r,\varphi,z) = v_0(r,\varphi) - z\vartheta_r(r,\varphi), \qquad w(r,\varphi,z) = w_0(r,\varphi) \tag{1}$$

where $\vartheta_r, \vartheta_\varphi$, defined over the middle surface, are the components of the infinitesimal rotation of the transverse material fibres about the unit radial and circumferential directions, respectively.

We admit that the environment interacts with the plates by contact on the outer surface and at a distance in the volume. If the outer actions and constraints are axisymmetric and we limit our study to linear elastic materials with axisymmetric distribution, the plate mechanical response shall also be axisymmetric: that is, all the fields of interest will not depend on the circumferential coordinate φ. Then, the infinitesimal three-dimensional components of longitudinal strain read

$$\varepsilon_{rr} = \frac{\partial u}{\partial r}, \qquad \varepsilon_{\varphi\varphi} = \frac{1}{r}\frac{\partial v}{\partial \varphi} + \frac{u}{r} = \frac{u}{r}, \qquad \varepsilon_{zz} = \frac{\partial w}{\partial z} = 0 \tag{2}$$

where, for the sake of simplicity of notation, the dependence on the independent variables was understood and hence omitted. Due to the Kirchhoff-Love inner constraint and the supposed axial symmetry, the infinitesimal three-dimensional components of shearing strain read

$$\gamma_{r\varphi} = \frac{1}{r}\frac{\partial u}{\partial \varphi} + \frac{\partial v}{\partial r} = \frac{\partial v}{\partial r}, \qquad \gamma_{rz} = \frac{\partial w}{\partial r} + \vartheta_\varphi = 0 \Longrightarrow \vartheta_\varphi = -\frac{dw_0}{dr},$$
$$\gamma_{\varphi z} = \frac{1}{r}\frac{\partial w}{\partial \varphi} - \vartheta_r = 0 \Longrightarrow \vartheta_r = 0 \tag{3}$$

That is, the rotation components $\vartheta_r, \vartheta_\varphi$ are nil (see Eq. (3-3)) and expressed in terms of the slope of the deflected middle surface (see Eq. (3-2)), respectively. The variation of the rotation of the transverse fibres along the plate provides the plate curvatures in the deformed shape:

$$\chi_{rr} = -\frac{\partial \vartheta_\varphi}{\partial r} = \frac{d^2 w}{dr^2}, \qquad \chi_{\varphi\varphi} = -\left(\frac{1}{r}\frac{\partial \vartheta_r}{\partial \varphi} + \frac{\vartheta_\varphi}{r}\right) = \frac{1}{r}\frac{dw}{dr}, \qquad \chi_{r\varphi} = -\frac{\partial \vartheta_r}{\partial r} + \frac{1}{r}\frac{\partial \vartheta_\varphi}{\partial \varphi} = 0 \tag{4}$$

By combining Eqs. (1)-(4) we obtain the non-vanishing deformation measures for the plate:

$$\varepsilon_{rr} = \frac{\partial u_0}{\partial r} - z\frac{d^2 w_0}{dr^2}, \qquad \varepsilon_{\varphi\varphi} = \frac{u_0}{r} - \frac{z}{r}\frac{dw_0}{dr}, \qquad \gamma_{r\varphi} = \frac{dv_0}{dr} \tag{5}$$

Let us pose that the material composing the plate is isotropic and linear elastic, non-homogeneous and functionally graded along both radial and transverse directions, though keeping Poisson's ratio ν uniform throughout the plate. Then, the constitutive relations for the plane state of strain exhibited by any lamina of the plate parallel to the middle surface read [35]

$$\sigma_{rr} = \frac{E(r,z)}{1-\nu^2}\left(\varepsilon_{rr} + \nu\varepsilon_{\varphi\varphi}\right) = \frac{E(r,z)}{1-\nu^2}\left[\left(\frac{du_0}{dr} + \nu\frac{u_0}{r}\right) - z\left(\frac{d^2 w_0}{dr^2} + \frac{\nu}{r}\frac{dw_0}{dr}\right)\right],$$
$$\sigma_{\varphi\varphi} = \frac{E(r,z)}{1-\nu^2}\left(\varepsilon_{\varphi\varphi} + \nu\varepsilon_{rr}\right) = \frac{E(r,z)}{1-\nu^2}\left[\left(\frac{u_0}{r} + \nu\frac{du_0}{dr}\right) - z\left(\frac{1}{r}\frac{dw_0}{dr} + \nu\frac{d^2 w_0}{dr^2}\right)\right], \tag{6}$$
$$\tau_{r\varphi} = \frac{E(r,z)}{2(1+\nu)}\gamma_{r\varphi} = \frac{E(r,z)}{2(1+\nu)}\frac{dv_0}{dr}$$

However, the supposed axial symmetry implies that the only component of the tangential stress that is constitutively prescribed shall vanish identically. Hence, Eq. (5-3) implies that the

displacement component v_0 must be uniform. This is impossible due to axial symmetry, though, thus the mechanics of the plate is well described by the kinematical fields $u_0(r), w_0(r)$, or, equivalently, by Eq. (3-2), $u_0(r), \vartheta_\varphi(r)$, describing the slab and transverse behaviour, respectively.

Let the functional grading admit a multiplicative representation, i.e., let Young's modulus be

$$E(r,z) = E_0 g(r) f(z), \qquad f(z) = f(-z) \tag{7}$$

where Eq. (7-2) translates the supposition that, with no restriction of generality, the functional grading is symmetrical with respect to the middle surface. The terms $g(r)$ and $f(z)$ are purely numerical, i.e., the physical dimensions of Young's modulus are retained in the reference value E_0.

The stress distributions provided by Eq. (6), once taken account of the functional grading in Eq. (7), are statically equivalent, due to the supposed rigidity of the transverse filaments, to the forces and moments per unit length of any line drawn on the middle surface given by [35]

$$\begin{aligned}
N_{rr} &= \int_{-\frac{h}{2}}^{\frac{h}{2}} \sigma_{rr}\, dz = \int_{-\frac{h}{2}}^{\frac{h}{2}} \frac{E(r,z)}{1-\nu^2}\left(\varepsilon_{rr} + \nu\varepsilon_{\varphi\varphi}\right) dz = \frac{E_0 g(r) \bar{f} h}{1-\nu^2}\left(\frac{du_0}{dr} + \nu\frac{u_0}{r}\right), \\
N_{\varphi\varphi} &= \int_{-\frac{h}{2}}^{\frac{h}{2}} \sigma_{\varphi\varphi}\, dz = \int_{-\frac{h}{2}}^{\frac{h}{2}} \frac{E(r,z)}{1-\nu^2}\left(\varepsilon_{\varphi\varphi} + \nu\varepsilon_{rr}\right) dz = \frac{E_0 g(r) \bar{f} h}{1-\nu^2}\left(\frac{u_0}{r} + \nu\frac{du_0}{dr}\right), \\
M_{rr} &= \int_{-\frac{h}{2}}^{\frac{h}{2}} -z\sigma_{rr}\, dz = \int_{-\frac{h}{2}}^{\frac{h}{2}} -z\frac{E(r,z)}{1-\nu^2}\left(\varepsilon_{rr} + \nu\varepsilon_{\varphi\varphi}\right) dz = \frac{E_0 g(r) \bar{\bar{f}} h^3}{12(1-\nu^2)}\left(\frac{d^2 w_0}{dr^2} + \frac{\nu}{r}\frac{dw_0}{dr}\right), \\
M_{\varphi\varphi} &= \int_{-\frac{h}{2}}^{\frac{h}{2}} -z\sigma_{\varphi\varphi}\, dz = \int_{-\frac{h}{2}}^{\frac{h}{2}} -z\frac{E(r,z)}{1-\nu^2}\left(\varepsilon_{rr} + \nu\varepsilon_{\varphi\varphi}\right) dz = \frac{E_0 g(r) \bar{\bar{f}} h^3}{12(1-\nu^2)}\left(\frac{1}{r}\frac{dw_0}{dr} + \nu\frac{d^2 w_0}{dr^2}\right)
\end{aligned} \tag{8}$$

In Eq. (8) the averages $\bar{f}, \bar{\bar{f}}$ are known quantities once the function $f(z)$ is given, in that

$$\bar{f} = \int_{-\frac{h}{2}}^{\frac{h}{2}} f(z)\, dz, \qquad \bar{\bar{f}} = \int_{-\frac{h}{2}}^{\frac{h}{2}} z^2 f(z)\, dz \tag{9}$$

Just to provide a couple of meaningful examples for Eq. (9), we have that, for a parabolic distribution equal to α at the bases and β at the middle surface,

$$f_1(z) = (\alpha - \beta)\left(\frac{2z}{h}\right)^2 + \beta \Longrightarrow \bar{f}_1 = \frac{\alpha + 2\beta}{3}, \qquad \bar{\bar{f}}_1 = \frac{3\alpha + 2\beta}{5}$$

For a co-sinusoidal distribution equal to α at the bases and β at the middle surface,

$$f_2(z) = (\beta - \alpha)\cos\left(\frac{\pi z}{h}\right) + \alpha \Longrightarrow \bar{f}_2 = \frac{2\beta + (\pi - 2)\alpha}{\pi}, \quad \bar{\bar{f}}_2 = \frac{6\beta(\pi^2 - 8) + \alpha(\pi^3 - 6\pi^2 + 48)}{\pi^3}$$

It is worth remarking that Eq. (8) provides the stress resultants that are constitutively prescribed, which turn out to be a function of the radial coordinate r only; yet, in general two other non-vanishing stress resultants appear, due to the reactions associated to the Kirchhoff-Love inner constraint of vanishing shearing strain:

$$Q_{zr} = \int_{-\frac{h}{2}}^{\frac{h}{2}} \tau_{zr}\, dz, \qquad Q_{\varphi r} = \int_{-\frac{h}{2}}^{\frac{h}{2}} \tau_{\varphi r}\, dz \tag{10}$$

Due to the postulated axial symmetry, however, the second shearing force component in Eq. (10) vanishes, but we must keep Q_{zr} to balance the outer distributed transverse force.

The local balance of slab forces in the radial direction reads, once posed b_r the resultant of the radial component of the outer volume force over the transverse filaments [35],

$$\frac{dN_{rr}}{dr} + \frac{N_{rr}}{r} - \frac{N_{\varphi\varphi}}{r} + b_r = 0 \tag{11}$$

while the balance in the circumferential direction is identically satisfied for axial symmetry. Then, inserting the first two Eq. (8) into Eq. (11) yields the field equation for the slab behaviour

$$\frac{dg(r)}{dr}\left[\frac{du_0(r)}{dr} + \nu\frac{u_0(r)}{r}\right] + g(r)\left[\frac{d^2u_0(r)}{dr^2} + \frac{1}{r}\frac{du_0(r)}{dr} - \frac{u_0(r)}{r^2}\right] + \frac{(1-\nu^2)b_r(r)}{E_0\bar{f}h} = 0 \tag{12}$$

that is in terms of the radial displacement component of the middle surface $u_0(r)$; Eq. (12) is ordinary since all functions depend on the radial variable only.

The local balance for the transverse force reads, if b_z denotes the resultant over the transverse filaments of the transverse component of the outer volume force and contact force at the bases [35],

$$\frac{dQ_{zr}}{dr}+\frac{Q_{zr}}{r}+b_z=0\Longrightarrow Q_{zr}(r)=Q_i-\frac{1}{r}\int_{r_i}^{r}\bar{r}b_z(\bar{r})d\bar{r} \tag{13}$$

where Q_i is the value attained at the inner radius; if the plate is solid, $r_i=0$ and $Q_i=0$.

By axial symmetry, $M_{\varphi\varphi}$ is uniform on any circle with the same centre of the boundaries of the middle surface; then, the local balance of moment about the radial direction is identically satisfied. On the other hand, the local balance of moment about the circumferential direction reads [35]

$$\frac{dM_{rr}}{dr}+\frac{M_{rr}}{r}-\frac{M_{\varphi\varphi}}{r}+Q_{zr}=0 \tag{14}$$

If the plate is solid, Eq. (13) provides the transverse shearing force to insert in Eq. (14), yielding

$$\begin{aligned}\frac{dg(r)}{dr}\left[r\frac{d\vartheta_\varphi(r)}{dr}+\nu\vartheta_\varphi(r)\right]+g(r)\left[r\frac{d^2\vartheta_\varphi(r)}{dr^2}+\frac{d\vartheta_\varphi(r)}{dr}-\frac{\vartheta_\varphi(r)}{r}\right]\\ =\frac{12\,(\nu^2-1)}{E_0\bar{\bar{f}}h^3}\int_0^r\bar{r}b_z(\bar{r})d\bar{r}\end{aligned} \tag{15}$$

If Q_i is not known in Eq. (13), it is useful to arrange Eqs. (13) and (14) in such a way to have only constitutively prescribed quantities, thus providing [35]

$$\frac{1}{r}\frac{d}{dr}\left[\frac{d(rM_{rr})}{dr}-M_{\varphi\varphi}\right]=b_z \tag{16}$$

Inserting the last two Eq. (8) into Eq. (16) yields the field equation for the transverse behaviour

$$\begin{aligned}\frac{d}{dr}\left\{\frac{dg(r)}{dr}\left[r\frac{d\vartheta_\varphi(r)}{dr}+\nu\vartheta_\varphi(r)\right]+g(r)\left[r\frac{d^2\vartheta_\varphi(r)}{dr^2}+\frac{d\vartheta_\varphi(r)}{dr}-\frac{\vartheta_\varphi(r)}{r}\right]\right\}\\ =\frac{12(\nu^2-1)rb_z(r)}{E_0\bar{\bar{f}}h^3}\end{aligned} \tag{17}$$

To abstract from specific values of the geometrical and mechanical properties of the plates, and to have an outlook on their general behaviour, it is customary to turn the governing equation into a non-dimensional form. On this purpose, we introduce the following non-dimensional quantities

$$\rho = \frac{r}{r_o}, \qquad \bar{u} = \frac{u_0}{r_o}, \qquad \bar{w} = \frac{w_0}{r_o}, \qquad \lambda = \frac{h}{r_0}, \qquad \bar{b}_r = \frac{(1-\nu^2)b_r}{E_0 \bar{f} \lambda}, \qquad \bar{b}_z = \frac{12(1-\nu^2)b_z}{E_0 \bar{\bar{f}} \lambda^3} \tag{18}$$

Inserting Eq. (18) in the governing Eqs. (12), (17) (or, when possible, into Eq. (15)), letting $\theta = \vartheta_\varphi$ and denoting by primes the derivatives of the indicated fields with respect to ρ, one obtains

$$\begin{gathered} g'\rho(\rho\bar{u}' + \nu\bar{u}) + g(\rho^2\bar{u}'' + \rho\bar{u}' - \bar{u}) + \rho^2\bar{b}_r = 0, \\ \{g'\rho(\rho\theta' + \nu\theta) + g(\rho^2\theta'' + \rho\theta' - \theta)\}' + \rho^2\bar{b}_z = 0, \end{gathered} \tag{19}$$

where all the indicated fields have now been turned into functions of ρ.

Eq. (19) represent the field equations for the non-dimensional behaviour of the plate, which should be supplemented by suitable boundary conditions. It is worth remarking that, since the functional grading is symmetric with respect to the middle surface, the ordinary boundary conditions for homogeneous plates, which refer to kinematical descriptors referred to the middle surface, or to contact actions reduced to poles lying on the middle surface, may still be considered.

In the following sections we will investigate the possibility to obtain closed-form solutions for both the slab and transverse behaviour, starting from simple, yet meaningful, functional grading along the radius; indeed, the effect of the functional grading along the thickness is summoned in the numerical factors $\bar{f}, \bar{\bar{f}}$. Remark that, due to the choice of θ as kinematical descriptor for the transverse behaviour, Eq. (19-2) is similar to its counterpart Eq. (19-1), thus implying that, if closed-form solutions can be found for the slab behaviour, it is possible to find them also for the transverse behaviour.

3. SLAB BEHAVIOUR

For the sake of simplicity, we will assume as reasonable from the point of view of applications that the in-plane external load $\bar{b}_r$ vanishes, and the plate is loaded only by a uniform radial contact force per unit length at the boundary. We will consider a couple of paradigmatic functional gradings and two meaningful structural schemes, that is, the simply supported solid plate and the hollow plate simply supported at the inner boundary.

If the functional grading is exponential, i.e., $g(\rho) = e^{\zeta\rho}$, ζ being a real number, it is immediate to check that Eq. (19-1) admits closed-form solution in terms of special functions. In particular, for a simply supported solid plate the boundary conditions are

$$\bar{u}(\rho)|_{\rho=0} = 0, \qquad g(\rho)\left[\bar{u}'(\rho) + \nu\frac{\bar{u}(\rho)}{\rho}\right]\Bigg|_{\rho=1} = \bar{N}, \qquad \bar{N} = \frac{(1-\nu^2)N_{ext}}{E_0\bar{f}h} \tag{20}$$

We remark that Eq. (20-1) derives from axial symmetry, while Eq. (20-2) is the natural boundary condition at the outer boundary, where the radial in-plane contact force per unit length N_{ext} is prescribed and expressed in a non-dimensional form according to Eq. (20-3).

Eqs. (19-1) and (20) admit the closed-form solution

$$\bar{u}(\rho) = \frac{e^{-\zeta\rho}\bar{N}\rho L^2_{\nu-2}(\zeta\rho)}{(1+\nu-\zeta)L^2_{\nu-2}(\zeta) - \zeta L^3_{\nu-3}(\zeta)} \tag{21}$$

where $L^a_n(x)$ is Laguerre generalised polynomial of order n with parameter a [36].

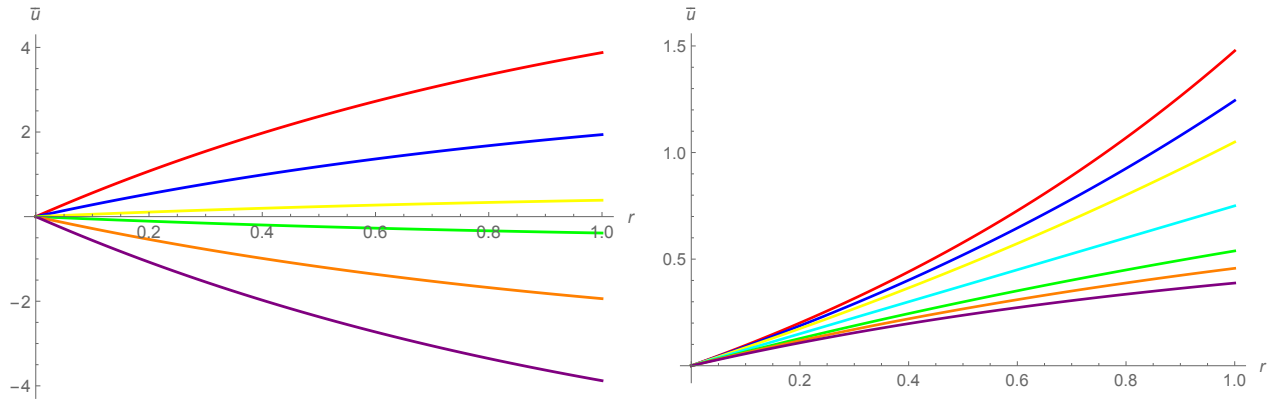

a) b)

Figure 1: non-dimensional radial displacement for Poisson's ratio $\nu = 1/3$ and a) coefficient of the functional grading $\zeta = 1$, variable applied load – Red, $\bar{N} = 10$, Blue, $\bar{N} = 5$, Yellow, $\bar{N} = 1$, Green, $\bar{N} = -1$, Orange, $\bar{N} = -5$, Purple, $\bar{N} = -10$; b) applied load $\bar{N} = 1$, variable coefficient of the functional grading – Red, $\zeta = -1$, Blue, $\zeta = -3/4$, Yellow, $\zeta = -1/2$, Cyan, $\zeta = 0$, Green, $\zeta = 1/2$, Orange, $\zeta = 3/4$, Purple, $\zeta = 1$.

In Fig. 1 we see a couple of graphs providing the non-dimensional radial displacement component $\bar{u}(\rho)$ for a given value $\nu = 1/3$ of Poisson's ratio; Fig. 1a) provides the curves corresponding to a fixed value $\zeta = 1$ and various values of the applied radial force per unit length at the boundary. We may see that for a given functional grading, exponentially stiffening the plate from the centre to the boundary, the radial displacement monotonically increases in absolute value and the plate behaves symmetrically in traction and compression, which is physically expected. Fig. 1b) provides the curves corresponding to a fixed value $\overline{N} = 1$ and various values of the coefficient of the exponential functional grading. We may see that negative coefficients of the exponential functional grading imply a remarkable softening effect (displacements are higher) with respect to no functional grading (cyan line), while positive coefficients imply a stiffening behaviour, which is physically expected.

We introduce a non-dimensional form for the in-plane radial and hoop contact forces per unit length (see also Eq. (20-3))

$$\overline{N}_{\rho\rho}(\rho) = \frac{N_{rr}(r_o\rho)(1-\nu^2)}{E_0\bar{f}h}, \qquad \overline{N}_{\varphi\varphi}(\rho) = \frac{N_{\varphi\varphi}(r_o\rho)(1-\nu^2)}{E_0\bar{f}h}, \tag{22-1}$$

Then, Eqs. (8), (18), (21) provide the closed-form expressions for $\overline{N}_{\rho\rho}(\rho), \overline{N}_{\varphi\varphi}(\rho)$ in terms of the external non-dimensional action $\overline{N}$ (see Eq. (20-3))

$$\begin{aligned} \overline{N}_{\rho\rho}(\rho) &= \frac{\overline{N}[\rho\zeta L^3_{\nu-3}(\zeta\rho) - (1+\nu-\zeta)L^2_{\nu-2}(\zeta\rho)]}{\zeta L^3_{\nu-3}(\zeta) - (1+\nu-\zeta)L^2_{\nu-2}(\zeta)}, \\ \overline{N}_{\varphi\varphi}(\rho) &= \frac{\overline{N}[\nu\rho\zeta L^3_{\nu-3}(\zeta\rho) - (1+\nu-\nu\zeta\rho)L^2_{\nu-2}(\zeta\rho)]}{\zeta L^3_{\nu-3}(\zeta) - (1+\nu-\zeta)L^2_{\nu-2}(\zeta)} \end{aligned} \tag{22-2}$$

The curves corresponding to these laws are represented in Fig. 2 for given values of Poisson's ratio and external load at the boundary, $\nu = 1/3, \overline{N} = 1$, and various values of the coefficient of the exponential functional grading. It is interesting to remark that a softening functional grading leads to a monotonically decreasing radial force along the non-dimensional radius, while the opposite holds for a hardening functional grading; no functional grading (cyan line) implies a uniform value for $\overline{N}_{\rho\rho}$, equal to the assigned one at the boundary. The curves for the circumferential contact force are not

trivial but always monotonic; they are decreasing for softening functional grading, increasing otherwise, and cross the cyan line, providing the uniform value corresponding to no functional grading, at points moving from centre to boundary as long as the functional grading hardens the plate. The behaviour in compression is symmetrical to the one presented in Figure 1, relative to traction, hence it will not be reported for the sake of brevity.

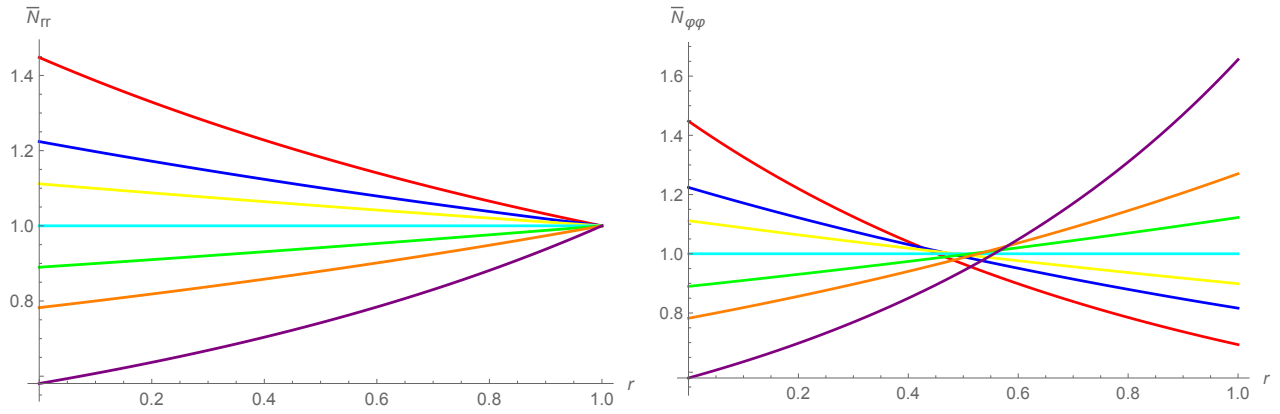

a) b)

Figure 2: non-dimensional radial a) and circumferential b) inner forces per unit length for Poisson's ratio $\nu = 1/3$ and external load $\bar{N} = 1$ for variable coefficient of the functional grading – Red, $\zeta = -2$, Blue, $\zeta = -1$, Yellow, $\zeta = -1/2$, Cyan, $\zeta = 0$, Green, $\zeta = 1/2$, Orange, $\zeta = 1$, Purple, $\zeta = 2$.

If the functional grading is exponential as above, for a hollow plate that is simply supported at the outer boundary and uniformly radially loaded at the inner boundary the boundary conditions are

$$g(\rho)\left[\bar{u}'(\rho) + \nu\frac{\bar{u}(\rho)}{\rho}\right]\Bigg|_{\rho=\frac{1}{5}} = \bar{N}, \qquad \bar{u}(\rho)|_{\rho=1} = 0 \tag{23}$$

where, just as an example, the boundary of the inner hole is a circle with radius one fifth of the outer boundary of the plate. The solutions for the non-dimensional in-plane displacement $\bar{u}(\rho)$ and contact forces per unit length $\bar{N}_{\rho\rho}(\rho), \bar{N}_{\varphi\varphi}(\rho)$ are found in closed form in terms of a coefficient Z

$$Z\bar{u}(\rho) = 5e^{-\zeta\rho}\bar{N}\rho[U(2-\nu,3,\zeta\rho)L^2_{\nu-2}(\zeta) - U(2-\nu,3,\zeta)L^2_{\nu-2}(\zeta\rho)], \tag{24}$$

$$Z\bar{N}_{\rho\rho}(\rho) = 5\bar{N}\{L^2_{\nu-2}(\zeta)[(1+\nu-\zeta\rho)U(2-\nu,3,\zeta\rho) - \zeta\rho(2-\nu)U(3-\nu,4,\zeta\rho)]$$

$$+ U(2-\nu,3,\zeta)[\zeta\rho L^3_{\nu-3}(\zeta\rho) - (1+\nu-\zeta\rho)L^2_{\nu-2}(\zeta\rho)]\},$$

$$Z\bar{N}_{\varphi\varphi}(\rho) = 5\bar{N}\{L^2_{\nu-2}(\zeta)[(1+\nu-\nu\zeta\rho)U(2-\nu,3,\zeta\rho) - \nu\zeta\rho(2-\nu)U(3-\nu,4,\zeta\rho)]$$

$$+ U(2-\nu,3,\zeta)[\nu\zeta\rho L^3_{\nu-3}(\zeta\rho) - (1+\nu-\nu\zeta\rho)L^2_{\nu-2}(\zeta\rho)]\},$$

$$Z = U(2-\nu,3,\zeta)\left[\zeta L^3_{\nu-3}\left(\frac{\zeta}{5}\right) - (5+5\nu-\zeta)L^2_{\nu-2}\left(\frac{\zeta}{5}\right)\right]$$

$$+ L^2_{\nu-2}(\zeta)\left[(5+5\nu-\zeta)U\left(2-\nu,3,\frac{\zeta}{5}\right) - \zeta(2-\nu)U\left(3-\nu,4,\frac{\zeta}{5}\right)\right]$$

where $U(a,b,x)$ is the so-called confluent hypergeometric function [37].

Fig. 3 shows, similarly to what is done in Fig. 1, the non-dimensional radial displacement component $\bar{u}(\rho)$ for Poisson's ratio $\nu = 1/3$; Fig. 3a) provides the curves corresponding to $\zeta = 1$ and variable applied radial force per unit length at the boundary. We may easily see the hardening and softening behaviour associated with the corresponding functional grading, thus reflecting physical intuition. Fig. 3b) provides the curves corresponding to $\bar{N} = 1$ and variable coefficient of the exponential functional grading. We may see that negative coefficients of the exponential functional grading imply a remarkable softening effect with respect to no functional grading (cyan line), while positive coefficients imply a stiffening behaviour, which is physically expected.

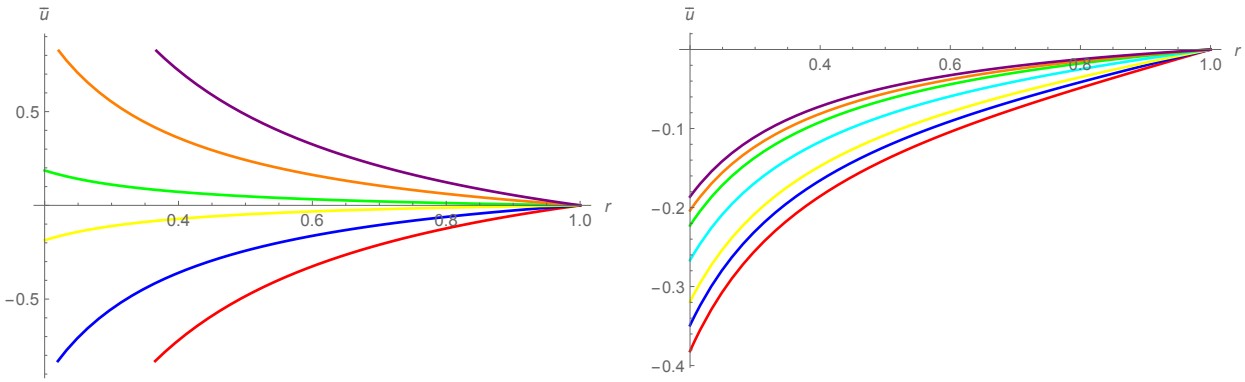

a) b)

Figure 3: non-dimensional radial displacement for Poisson's ratio $\nu = 1/3$ and a) coefficient of the functional grading $\zeta = 1$, variable applied load – Red, $\bar{N} = 10$, Blue, $\bar{N} = 5$, Yellow, $\bar{N} = 1$, Green, $\bar{N} = -1$, Orange, $\bar{N} = -5$, Purple,

$\bar{N} = -10$; b) applied load $\bar{N} = 1$, variable coefficient of the functional grading – Red, $\zeta = -1$, Blue, $\zeta = -3/4$, Yellow, $\zeta = -1/2$, Cyan, $\zeta = 0$, Green, $\zeta = 1/2$, Orange, $\zeta = 3/4$, Purple, $\zeta = 1$.

Fig. 4 presents the non-dimensional radial and hoop normal forces per unit length for $\nu = 1/3, \bar{N} = 1$, and various values of the coefficient of the exponential functional grading.

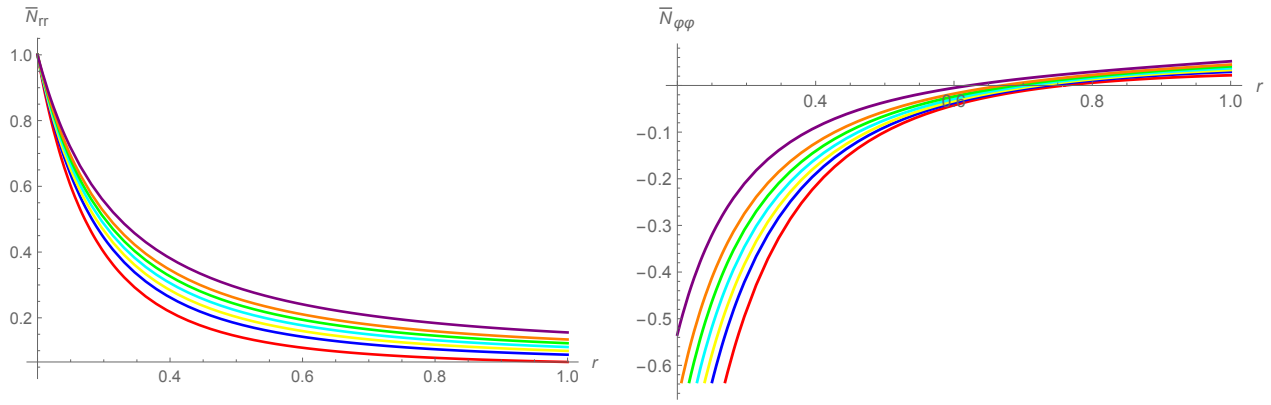

a) b)

Figure 4: non-dimensional radial a) and circumferential b) inner forces per unit length for Poisson's ratio $\nu = 1/3$ and external load $p = 1$ for variable coefficient of the functional grading – Red, $\zeta = -2$, Blue, $\zeta = -1$, Yellow, $\zeta = -1/2$, Cyan, $\zeta = 0$, Green, $\zeta = 1/2$, Orange, $\zeta = 1$, Purple, $\zeta = 2$.

The radial force monotonically decreases along the radius, as for homogeneous plates (cyan lines); for a softening functional grading, the values of the radial force are lower than for the homogeneous plate, while the opposite holds for hardening functional grading: this is in accord with physical intuition. The hoop force monotonically increases along the radius, as for homogeneous plates (cyan lines); the behaviour for different functional grading follows physical intuition.

If the functional grading is polynomial, i.e., $g(\rho) = (1+\rho)^{\zeta}$, ζ being a real number, it is immediate to check that Eq. (19-1) provides closed-form solutions for the non-dimensional in-plane displacement $\bar{u}(\rho)$ and contact forces per unit length $\bar{N}_{\rho\rho}(\rho), \bar{N}_{\varphi\varphi}(\rho)$ in terms of a coefficient W

$$W\bar{u}(\rho) = 3\,2^{-\zeta}\bar{N}\rho\left[{}_2F_1\left(\frac{1}{2}\left(2+\zeta-\sqrt{4+\zeta^2-4\nu\zeta}\right),\frac{1}{2}\left(2+\zeta+\sqrt{4+\zeta^2-4\nu\zeta}\right),3,-\rho\right)\right], \quad (25)$$

$$W\bar{N}_{\rho\rho}(\rho) = \bar{N}(1+\rho)^{\zeta}\left[{}_3F_1\left(1+\frac{\zeta}{2}-\sqrt{1+\frac{\zeta^2}{4}-\nu\zeta},1+\frac{\zeta}{2}+\sqrt{1+\frac{\zeta^2}{4}-\nu\zeta},3,-\rho\right)\right.$$

$$\left.-\zeta\rho\,{}_2F_1\left(1+\frac{\zeta}{2}-\sqrt{1+\frac{\zeta^2}{4}-\nu\zeta},1+\frac{\zeta}{2}+\sqrt{1+\frac{\zeta^2}{4}-\nu\zeta},4,-\rho\right)\right],$$

$$W\bar{N}_{\varphi\varphi}(\rho) = \bar{N}(1+\rho)^{\zeta}\left[{}_3F_1\left(1+\frac{\zeta}{2}-\sqrt{1+\frac{\zeta^2}{4}-\nu\zeta},1+\frac{\zeta}{2}+\sqrt{1+\frac{\zeta^2}{4}-\nu\zeta},3,-\rho\right)\right.$$

$$\left.-\nu\zeta\rho\,{}_2F_1\left(1+\frac{\zeta}{2}-\sqrt{1+\frac{\zeta^2}{4}-\nu\zeta},1+\frac{\zeta}{2}+\sqrt{1+\frac{\zeta^2}{4}-\nu\zeta},4,-\rho\right)\right],$$

$$W = (1+\nu)\left[{}_2F_1\left(1+\frac{\zeta}{2}-\sqrt{1+\frac{\zeta^2}{4}-\nu\zeta},1+\frac{\zeta}{2}+\sqrt{1+\frac{\zeta^2}{4}-\nu\zeta},3,-1\right)\right.$$

$$\left.-\zeta\,{}_2F_1\left(1+\frac{\zeta}{2}-\sqrt{1+\frac{\zeta^2}{4}-\nu\zeta},1+\frac{\zeta}{2}+\sqrt{1+\frac{\zeta^2}{4}-\nu\zeta},4,-1\right)\right],$$

where ${}_2F_1(a,b,c,z)$ is the hypergeometric function [38].

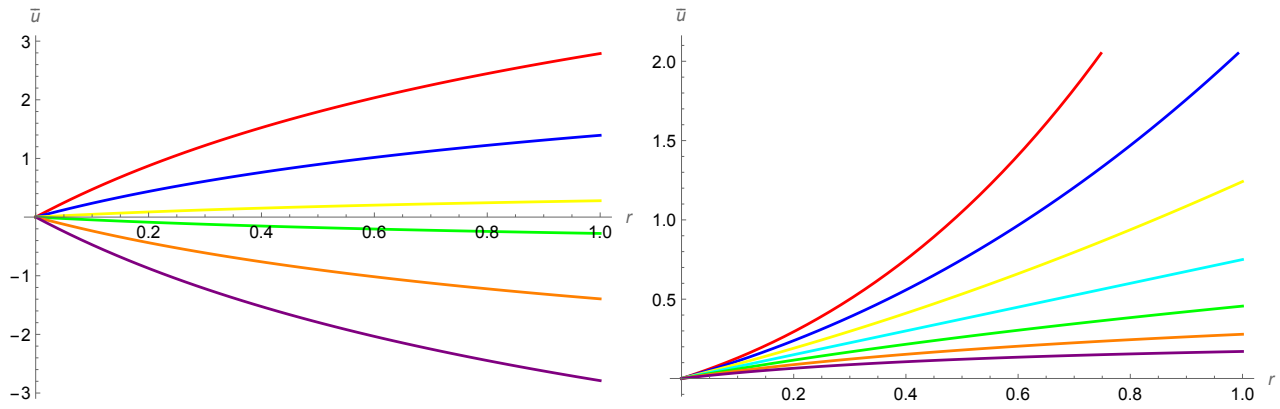

a) b)

Figure 5: non-dimensional radial displacement for Poisson's ratio $\nu = 1/3$ and a) coefficient of the functional grading $\zeta = 2$, variable applied load – Red, $\bar{N} = 10$, Blue, $\bar{N} = 5$, Yellow, $\bar{N} = 1$, Green, $\bar{N} = -1$, Orange, $\bar{N} = -5$, Purple, $\bar{N} = -10$; b) applied load $\bar{N} = 1$, variable coefficient of the functional grading – Red, $\zeta = -3$, Blue, $\zeta = -2$, Yellow, $\zeta = -1$, Cyan, $\zeta = 0$, Green, $\zeta = 1$, Orange, $\zeta = 2$, Purple, $\zeta = 3$.

Fig. 5 shows the non-dimensional radial displacement component $\bar{u}(\rho)$ for Poisson's ratio $\nu = 1/3$; Fig. 5a) provides the curves corresponding to $\zeta = 1$ and variable applied radial force per unit length at the boundary. The curves monotonically increase in absolute value; the hardening and softening behaviour associated with the corresponding functional grading reflects physical intuition. Fig. 5b) provides the curves corresponding to $\bar{N} = 1$ and variable exponent of the functional grading. All curves monotonically increase but their curvature is influenced by the exponent of the functional grading; moreover, negative ζ imply a remarkable softening effect with respect to no functional grading (cyan line), while positive ζ imply a physically expected stiffening behaviour.

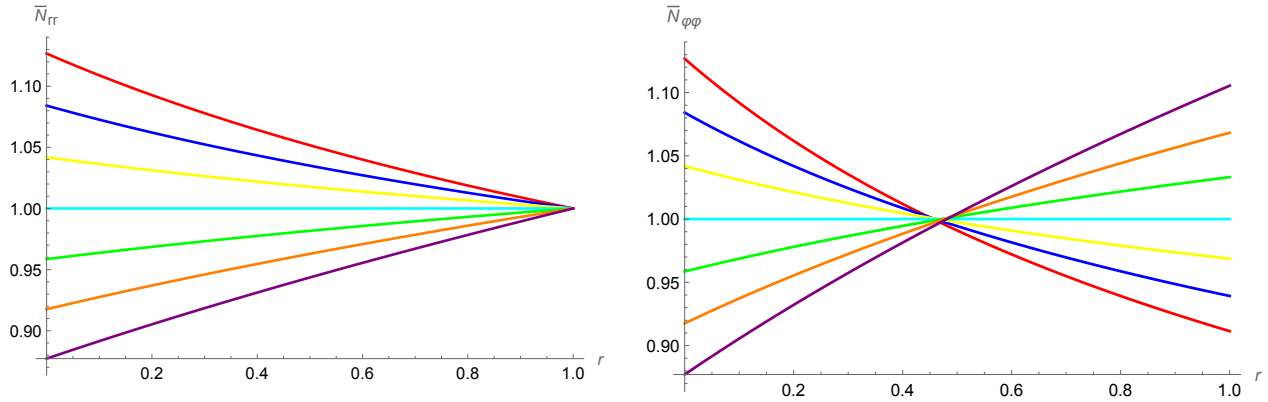

a) b)

Figure 6: non-dimensional radial a) and circumferential b) inner forces per unit length for Poisson's ratio $\nu = 1/3$ and external load $\bar{N} = 1$ for variable coefficient of the functional grading – Red, $\zeta = -3/4$, Blue, $\zeta = -1/2$, Yellow, $\zeta = -1/4$, Cyan, $\zeta = 0$, Green, $\zeta = 1/4$, Orange, $\zeta = 1/2$, Purple, $\zeta = 3/4$.

Fig. 6 presents the non-dimensional radial and hoop normal forces per unit length for $\nu = 1/3, \bar{N} = 1$, and various values of the exponent of the functional grading. The radial force monotonically decreases along the radius for a softening functional grading, and the values of the radial force are lower than for the homogeneous plate; the opposite holds for hardening functional grading, in accord with physical intuition. The hoop force behaves similarly, and all curves meet at approximately one half of the radius.

Closed form solutions are at ease also for a hollow plate with the polynomial functional grading $g(\rho) = (1+\rho)^{\zeta}$, but their expression in terms of special functions (hypergeometric and Meijer) is rather cumbersome and will not be reported here for the sake of space.

4. TRANSVERSE BEHAVIOUR

For the sake of simplicity, we will assume that the transverse external load $\bar{b}_z$ assumes very simple expressions, that is, vanishing and uniform. We will consider a couple of paradigmatic functional gradings and simply supported solid and hollow plates.

Let us start with a solid plate; the functional grading be exponential, i.e., $g(\rho) = e^{\zeta\rho}$, ζ being real. If the applied load is a uniform couple at the outer boundary, the boundary conditions are

$$\theta(\rho)|_{\rho=0} = 0, \qquad -g(\rho)\left[\theta'(\rho) + \nu\frac{\theta(\rho)}{\rho}\right]\Bigg|_{\rho=1} = \bar{M}, \qquad \bar{M} = \frac{12(1-\nu^2)M_{ext}}{E_0\bar{\bar{f}}\lambda^3 r_0^2} \tag{26}$$

We remark that Eq. (26-1) derives from axial symmetry, while Eq. (26-2) is the natural boundary condition at the outer boundary, where the contact couple per unit length M_{ext} is prescribed and expressed in a non-dimensional form according to Eq. (26-3).

The differential Eq. (19-2) admits a trivial first integration for $\bar{b}_z = 0$, providing a constant of integration that must vanish due to its meaning of shearing force, balancing no external transverse load. Then, the solution of Eqs. (19-2), (26) is

$$\theta(\rho) = -\frac{e^{-\zeta\rho}\bar{M}\rho L^2_{\nu-2}(\zeta\rho)}{(1+\nu-\zeta)L^2_{\nu-2}(\zeta) - \zeta L^3_{\nu-3}(\zeta)} \tag{27}$$

which is similar to Eq. (21); its behaviour is shown in Fig. 7, which provides graphs of $\theta(\rho)$ for Poisson's ratio $\nu = 1/3$.

Fig. 7a) provides the curves corresponding to a fixed value $\zeta = 1/4$ and various values of the applied radial couple per unit length at the boundary. The given functional grading, exponentially stiffening the plate from the centre to the boundary, yields a rotation of the transverse fibres that

monotonically increases in absolute value and the plate behaves symmetrically for clockwise and anti-clockwise applied couples, which is physically expected. Fig. 7b) provides the curves corresponding to a fixed value $\bar{M} = 1$ and various values of the coefficient of the exponential functional grading. Negative values yield a softening effect (rotations are higher) with respect to no functional grading (green line), while positive coefficients imply the opposite, as physically expected.

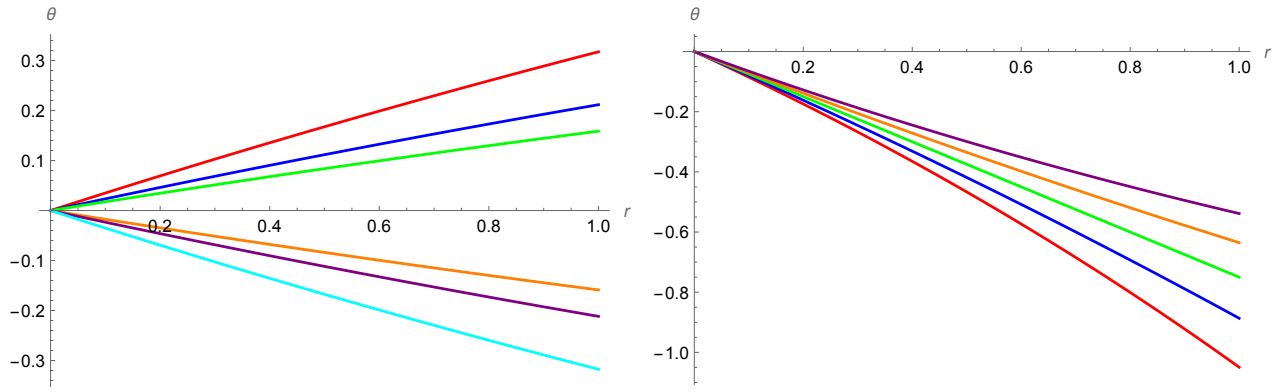

a) b)

Figure 7: transverse fibre rotation for Poisson's ratio $\nu = 1/3$ and a) coefficient of the functional grading $\zeta = 1/4$, variable applied couple – Red, $\bar{M} = -1/4$, Blue, $\bar{M} = -1/3$, Green, $\bar{M} = -1/2$, Orange, $\bar{M} = 1/4$, Purple, $\bar{M} = 1/3$, Cyan, $\bar{M} = 1/2$; b) applied couple $\bar{M} = 1$, variable coefficient of the functional grading – Red, $\zeta = -1/2$, Blue, $\zeta = -1/4$, Green, $\zeta = 0$, Orange, $\zeta = 1/4$, Purple, $\zeta = 1/2$.

Eq. (8), (18), (27) provide the closed-form expressions of the non-dimensional in-plane contact forces per unit length, absolutely analogous to those in Eq. (22),

$$\bar{M}_{\rho\rho}(\rho) = \frac{\bar{M}[\rho\zeta L^3_{\nu-3}(\zeta\rho) - (1+\nu-\zeta)L^2_{\nu-2}(\zeta\rho)]}{\zeta L^3_{\nu-3}(\zeta) - (1+\nu-\zeta)L^2_{\nu-2}(\zeta)}, \qquad \bar{M}_{\rho\rho}(\rho) = \frac{12(1-\nu^2)M_{rr}(r_o\rho)}{E_0\bar{\bar{f}}\lambda^3 r_0^2},$$
$$\bar{M}_{\varphi\varphi}(\rho) = \frac{\bar{M}[\nu\rho\zeta L^3_{\nu-3}(\zeta\rho) - (1+\nu-\nu\zeta\rho)L^2_{\nu-2}(\zeta\rho)]}{\zeta L^3_{\nu-3}(\zeta) - (1+\nu-\zeta)L^2_{\nu-2}(\zeta)}, \qquad \bar{M}_{\varphi\varphi}(\rho) = \frac{12(1-\nu^2)M_{\varphi\varphi}(r_o\rho)}{E_0\bar{\bar{f}}\lambda^3 r_0^2} \tag{28}$$

The curves corresponding to these laws are represented in Fig. 8 for given values of Poisson's ratio and external load at the boundary, $\nu = 1/3, \bar{M} = 1$, and various values of the coefficient of the exponential functional grading. The comments are analogous to those for Fig. 2.

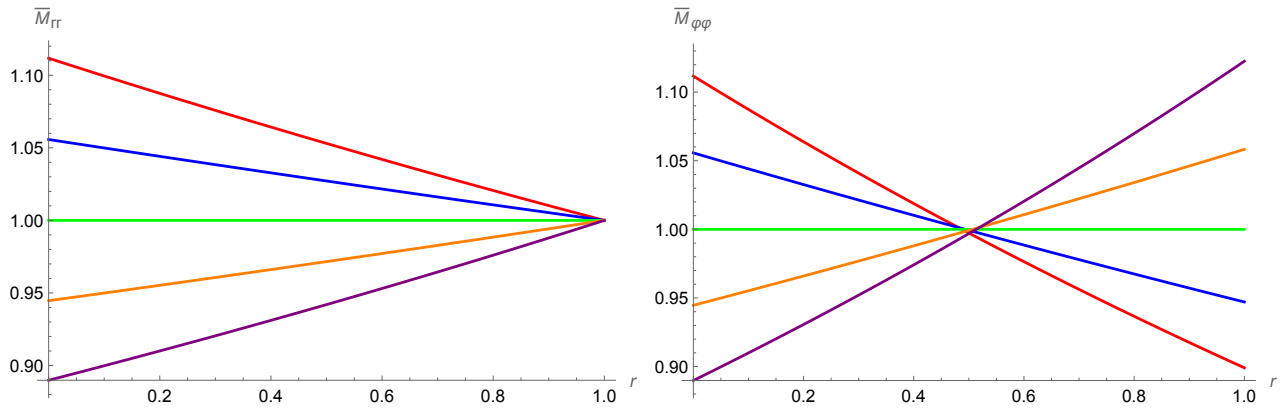

a) b)

Figure 8: non-dimensional radial a) and circumferential b) inner couples per unit length for Poisson's ratio $\nu = 1/3$ and external couple $\overline{M} = 1$ for variable coefficient of the functional grading – Red, $\zeta = -1/2$, Blue, $\zeta = -1/4$, Green, $\zeta = 0$, Green, $\zeta = 1/4$, Orange, $\zeta = 1/4$, Purple, $\zeta = 1/2$.

If the functional grading is polynomial, i.e., $g(\rho) = (1+\rho)^{\zeta}$, ζ real, Eq. (19-2) and Eq. (26) admit closed-form solutions in the same form as Eq. (25), just like Eq. (27) and (28) resemble their counterparts Eq. (21) and (22) for the slab behaviour, for the already mentioned correspondence between slab and transverse filed equations in this case.

5. CONCLUSION

In this study we furnished several closed-form solutions for functionally graded circular plates with variation of Young's elastic modulus in both radial and thickness directions. We postulated a multiplicative representation of the above quoted elastic modulus. Several special functions have been employed to accomplish this task. As the Refs. [39-46] suggest, there are relationships between axisymmetric bending, vibration and buckling solutions of FGM circular plates, based on higher-order plate theory and classical plate theory. Hence, a generalization of this work to encompass dynamic and stability problems, plus resorting to refined theories can be conducted in the future, along with related topics of buckling and vibration.

ACKNOWLEDGEMENTS

G. Ruta gratefully acknowledges the support of the institutional grant RM12017294D1B7EF of the university of Rome "La Sapienza" and of the PRIN grant 20177TTP3S_006 of the Italian Ministry of Research.

REFERENCES

[1] Garabedian C.A., Circular plates of constant or variable thickness, *Transactions of the American Mathematical Society* 25(3):343-398, 1923, DOI: 10.2307/1989296.

[2] Kitover K.A., *Circular Thin Plates,* Moscow: State Publishing in Architecture, 1953 (in Russian).

[3] Kovalenko A.D., Circular Variable-Thickness Plates, Moscow: "Fitzmatgiz" Publishers, 1959 (in Russian).

[4] Birger I.A., *Circular Plates and Shells of Revolution,* 1961 (in Russian).

[5] Gran Olsson R., Biegung kreisförmiger Plätte von radial veränderlicher Dicke, *Ingenieur-Archiv* 8:81-98, 1937 (in German).

[6] Bisshopp K.E., Lateral bending of symmetrically loaded conical discs, *Quarterly of applied mathematics* 2(3):205-217, 1944.

[7] Ando T., Bending Stress in Symmetrically Loaded Circular Plates, *Transactions of the Japanese society of mechanical engineers* 22(119):457-461, 1956.

[8] Lord H.W., Yousef S.S., Elastic bending of circular plates of variable thickness: an analytical and experimental study, *International Journal of Mechanical Sciences* 12(5):417-434, 1970, DOI: 10.1016/0020-7403(70)90104-9.

[9] Biswas P., Thermal deflection of an elastic circular plate of variable thickness, *Proceedings of the Indian Academy of Sciences-Section A* 85(1):1-7, Springer India, 1977.

[10] Laura P.A.A., Filipich C., Santos R.D., Static and dynamic behavior of circular plates of variable thickness elastically restrained along the edges, *Journal of Sound and Vibration* 52(2):243-251, 1977, DOI: 10.1016/0022-460X(77)90643-5.

[11] Han J-B., Liew K.M., The differential quadrature element method (DQEM) for axisymmetric bending of thick circular plates, in *3rd Asian-Pacific Conference on Computational Mechanics, Seoul, Korea*, 2363-2368, 1996.

[12] Reddy J.N., Wang C.M., Kitipornchai S., Axisymmetric bending of functionally graded circular and annular plates, *European Journal of Mechanics-A/Solids* 18(2):185-199, 1999, DOI: 10.1016/S0997-7538(99)80011-4.

[13] Civalek O., Ülker M., Harmonic differential quadrature (HDQ) for axisymmetric bending analysis of thin isotropic circular plates, *Structural Engineering and Mechanics* 17(1):1-14, 2004, DOI: 10.12989/sem.2004.17.1.001.

[14] Gunes R., Aydin M., Elastic response of functionally graded circular plates under a drop-weight, *Composite Structures* 92:2445–2456, 2010, DOI: 10.1016/j.compstruct.2010.02.015.

[15] Farahani B.V., Berardo J.M., Degas R., César de Sá J.M., Ferreira A.J., Belinha J., The axisymmetric analysis of circular plates using the radial point interpolation method, *International Journal for Computational Methods in Engineering Science and Mechanics* 16(6):336-353, 2015, DOI: 10.1080/15502287.2015.1103819.

[16] Tseng W.D., Tarn J.Q., Exact elasticity solution for axisymmetric deformation of circular plates, *Journal of Mechanics* 31(6):617-629, 2015, DOI: 10.1017/jmech.2015.37.

[17] Karttunen A.T., von Hertzen R., Reddy J.N., Romanoff J., Exact elasticity-based finite element for circular plates, *Computers & Structures* 182:219-226, 2017, DOI: 10.1016/j.compstruc.2016.11.013.

[18] Shariyat M., Alipour M.M., Analytical bending and stress analysis of variable thickness FGM auxetic conical/cylindrical shells with general tractions, *Latin American Journal of Solids and Structures* 14(5):805-843, 2017, DOI: 10.1590/1679-78253413.

[19] Saidi A.R., Rasouli A., Sahraee S., Axisymmetric bending and buckling analysis of thick functionally graded circular plates using unconstrained third-order shear deformation plate theory, *Composite Structures* 89(1):110-119, 2009, DOI: 10.1016/J.COMPSTRUCT.2008.07.003.

[20] Vivio F., Vullo V., Closed form solutions of axisymmetric bending of circular plates having non-linear variable thickness, *International Journal of Mechanical Sciences* 52(9):1234-1252, 2010, DOI: 10.1016/j.ijmecsci.2010.05.011.

[21] Alibeigloo A., Simintan V., Elasticity solution of functionally graded circular and annular plates integrated with sensor and actuator layers using differential quadrature, *Composite Structures* 93(10):2473-2486, 2011, DOI: 10.1016/j.compstruct.2011.04.003.

[22] Rad A.B., Behravan A., Static analysis of non-uniform 2D functionally graded auxetic-porous circular plates inter-acting with the gradient elastic foundations involving friction force, *Aerospace Science and Technology* 76:315-339, 2018, DOI: 10.12989/sem.2017.64.5.591.

[23] Yang Y., Zhang Y., Chen W., Yang B., On asymmetric bending of functionally graded solid circular plates, *Applied Mathematics and Mechanics* 39(6):767-782, 2018, DOI: 10.1007/s10483-018-2337-7.

[24] Belardi V.G., Fanelli P., Vivio F., Bending analysis with Galerkin method of rectilinear orthotropic composite circular plates subject to transversal load, *Composites Part B: Engineering* 140:250-259, 2018, DOI: 10.1016/j.compositesb.2017.12.011.

[25] Belardi V.G., Fanelli P., Vivio F., Elastic analysis of rectilinear orthotropic composite circular plates subject to transversal and in-plane load conditions using Ritz method, *Composite Structures* 199:63-75, 2018, DOI: 10.1016/J.COMPSTRUCT.2018.05.062.

[26] Belardi V.G., Fanelli P., Vivio F., Ritz method analysis of rectilinear orthotropic composite circular plates undergoing in-plane bending and torsional moments, *Mechanics of Advanced Materials and Structures* 28(9):963-979, 2021, DOI: 10.1080/15376494.2019.1614701.

[27] Magnucka-Blandzi E., Magnucki K., Stawecki W., Bending and buckling of a circular plate with symmetrically varying mechanical properties, *Applied Mathematical Modelling* 89:1198-1205, 2021, DOI: 10.1016/j.apm.2020.07.031.

[28] Hale J.S., Brunetti M., Bordas S.P.A., Maurini C., Simple and extensible plate and shell finite element models through automatic code generation tools, *Computers and Structures* 209:163-181, 2018, DOI: 10.1016/j.compstruc.2018.08.001.

[29] Elishakoff I., Pentaras D., Gentilini C., Mechanics of functionally graded material structures, Singapore: World Scientific, 2014.

[30] Gilat R., Caliò I., Elishakoff I., Inhomogeneous beams possessing an exponential mode shape, *Mechanics Research Communications* 37(4):417-426, 2010, DOI: 10.1016/j.mechrescom.2010.04.003.

[31] Ruta G., Elishakoff I., Suitable radial grading may considerably increase buckling loads of FGM circular plates, *Acta Mechanica* 229:2477–2493, 2018, DOI: 10.1007/s00707-017-2095-x

[32] Fiorini A., Ruta, G., Buckling of circular plates with functional grading in two directions, *Meccanica* 56:245–252, 2021, DOI: 10.1007/s11012-021-01306-6.

[33] K. Ichikawa (ed.), Functionally graded materials in the 21st century: a workshop on trends and forecasts. New York: Springer Science & Business Media, 2001.

[34] Miyamoto Y., Kaysser W., Rabin B., Kawasaki A., Ford R.G., Functionally graded materials: design, processing and applications, Materials Technology Series, volume 5. New York: Springer Science & Business Media, 2013.

[35] Timoshenko S.P., Woinowsky-Krieger S., *Theory of plates and shells* 2nd ed., New York: McGraw-Hill, 1959.

[36] Koornwinder T.H. *et al.*, Orthogonal Polynomials. In: Digital library of mathematical functions, https://dlmf.nist.gov/18, updated Sept. 15, 2020.

[37] Olde Daalhuis A.B., Confluent hypergeometric functions. In: Digital library of mathematical functions, https://dlmf.nist.gov/13, updated Sept. 15, 2020.

[38] Olde Daalhuis A.B., Hypergeometric function. In: Digital library of mathematical functions, https://dlmf.nist.gov/15, updated Sept. 15, 2020.

[39] Ma L.S., Wang T.J., Relationships between axisymmetric bending and buckling solutions of FGM circular plates based on third-order plate theory and classical plate theory, *International Journal of Solids and Structures* 41(1):85-101, 2004, DOI: 10.1016/j.ijsolstr.2003.09.008.

[40] Pardoen G.C., Deflection function for the symmetrical bending of circular plates, *AIAA Journal* 10(2):239-240, 1972, DOI: 10.2514/3.6571.

[41] Reiss E.L., A uniqueness theorem for the nonlinear axisymmetric bending of circular plates, *AIAA Journal* 1(11):2650-2651, 1963, DOI: 10.2514/3.2142.

[42] Lehnhoff T.F., Miller R.E., Influence of transverse shear on the small displacement theory of circular plates, *AIAA Journal* 7(8):1499-1505, 1969, DOI: 10.2514/3.5422.

[43] Stahl B., Keer L.M., Bending of a uniformly loaded circular plate with mixed boundary conditions, *AIAA Journal* 10(6):739-743, 1972, DOI: 10.2514/3.50204.

[44] Reddy J.N., Wang C.M., Relationships between classical and shear deformation theories of axisymmetric circular plates, *AIAA Journal* 35(12): 1862-1868, 1997, DOI: 10.2514/2.62.

[45] Leissa A.W., Clausen W.E., Deflection of a circular plate having mixed boundary conditions, *AIAA Journal* 5(12): 2287-2288, 1967, DOI: 10.2514/3.4432.

[46] Kao J.S., Bending of circular sandwich plates due to asymmetric temperature distribution, *AIAA Journal* 8(5):951-954, 1970, DOI: 10.2514/3.5800.